Bioactive Materials 34 (2024) 125–137

Contents lists available at ScienceDirect

Bioactive Materials

journal homepage: www.keaipublishing.com/en/journals/bioactive-materials

Systematic development of ionizable lipid nanoparticles for placental mRNA delivery using a design of experiments approach

Rachel E. Young [a,b], Katherine M. Nelson [c], Samuel I. Hofbauer [a,b,d], Tara Vijayakumar [a,b], Mohamad-Gabriel Alameh [e], Drew Weissman [e], Charalampos Papachristou [f], Jason P. Gleghorn [g], Rachel S. Riley [a,b,*]

[a] Department of Biomedical Engineering, Henry M. Rowan College of Engineering, Rowan University, 201 Mullica Hill Rd, Glassboro, NJ 08028, United States
[b] School of Translational Biomedical Engineering & Sciences, Virtua College of Medicine & Life Sciences of Rowan University, 201 Mullica Hill Rd, Glassboro, NJ 08028, United States
[c] Department of Chemical and Biomolecular Engineering, College of Engineering, University of Delaware, 150 Academy Street, Newark, DE 19716, United States
[d] Cooper Medical School of Rowan University, Rowan University, 401 Broadway, Camden, NJ 08103, United States
[e] Perelman School of Medicine, University of Pennsylvania, 3400 Civic Center Blvd, Philadelphia, PA 19104, United States
[f] Department of Mathematics, College of Science & Mathematics, Rowan University, 201 Mullica Hill Rd, Glassboro, NJ 08028, United States
[g] Department of Biomedical Engineering, College of Engineering, University of Delaware, 590 Avenue 1743, Newark, DE 19713, United States

ARTICLE INFO

Keywords:
Lipid nanoparticles (LNPs)
Drug delivery
Nucleic acids
Placental growth factor (PlGF)
Placenta
Pregnancy
Preeclampsia

ABSTRACT

Ionizable lipid nanoparticles (LNPs) have gained attention as mRNA delivery platforms for vaccination against COVID-19 and for protein replacement therapies. LNPs enhance mRNA stability, circulation time, cellular uptake, and preferential delivery to specific tissues compared to mRNA with no carrier platform. However, LNPs are only in the beginning stages of development for safe and effective mRNA delivery to the placenta to treat placental dysfunction. Here, we develop LNPs that enable high levels of mRNA delivery to trophoblasts *in vitro* and to the placenta *in vivo* with no toxicity. We conducted a Design of Experiments to explore how LNP composition, including the type and molar ratio of each lipid component, drives trophoblast and placental delivery. Our data revealed that utilizing C12-200 as the ionizable lipid and 1,2-dioleoyl-*sn*-glycero-3-phosphoethanolamine (DOPE) as the phospholipid in the LNP design yields high transfection efficiency *in vitro*. Analysis of lipid molar composition as a design parameter in LNPs displayed a strong correlation between apparent pKa and poly (ethylene) glycol (PEG) content, as a reduction in PEG molar amount increases apparent pKa. Further, we present one LNP platform that exhibits the highest delivery of placental growth factor mRNA to the placenta in pregnant mice, resulting in synthesis and secretion of a potentially therapeutic protein. Lastly, our high-performing LNPs have no toxicity to both the pregnant mice and fetuses. Our results demonstrate the feasibility of LNPs as a platform for mRNA delivery to the placenta, and our top LNP formulations may provide a therapeutic platform to treat diseases that originate from placental dysfunction during pregnancy.

1. Introduction

Recent developments in mRNA therapeutics include protein replacement therapies and vaccines, including two of the leading vaccine platforms against SARS-CoV-2 [1–7]. mRNA is a potent therapeutic tool because it enables transient protein production, limiting off-target and long-term effects that may occur with permanent gene editing technologies [8]. However, mRNA is easily degraded by serum endonucleases, and the negative charge of mRNA precludes their cellular entry [9]. Thus, various approaches to engineering novel mRNA delivery vehicles have emerged to promote high transfection and low toxicity [10]. Here, our goal is to develop a translational platform for mRNA delivery to the placenta to treat diseases of pregnancy.

In this work, we develop ionizable lipid nanoparticles (LNPs) as a platform for mRNA delivery to the placenta. The clinical use of LNPs has advanced tremendously over the past few years, and they are approved

Peer review under responsibility of KeAi Communications Co., Ltd.
* Corresponding author. 201 Mullica Hill Rd, Glassboro, NJ, 08028.United States.
E-mail address: rileyr@rowan.edu (R.S. Riley).

https://doi.org/10.1016/j.bioactmat.2023.11.014
Received 23 May 2023; Received in revised form 20 November 2023; Accepted 20 November 2023

by the FDA for vaccination against SARS-CoV-2 [11,12] and treatment of hereditary transthyretin amyloidosis [13,14]. Further, LNPs have undergone extensive preclinical and clinical research for the treatment of viral infections, genetic disorders, cancers, and more, making LNPs a highly translatable technology [9,15]. However, the development and study of LNPs in the field of maternal-fetal medicine has only recently begun to be explored [16,17].

LNPs are comprised of ionizable lipids, phospholipids, cholesterol, and lipid-conjugated poly (ethylene) glycol (PEG) that complex together to form spherical and multilamellar LNPs [18]. In acidic pH environments, such as intracellular endosomes, the ionizable lipids become positively charged, making LNPs highly efficient for endosomal escape and cytosolic nucleic acid delivery [19]. The functional roles of the phospholipid include bilayer formation and membrane fusion to promote LNP stabilization and endosomal escape, respectively [20,21]. Cholesterol affects LNP membrane rigidity, which increases encapsulation and reduces leakage of nucleic acids within the LNP [22]. The PEG-lipid conjugates increase LNP stability *in vitro* and reduce serum protein opsonization [23]. Altering the physicochemical properties and composition of LNPs, including the type and amount of each component, strongly influences their delivery to specific tissues and cells [24–27]. This dependence on LNP composition is due in large part to surface charge and pKa, which alters LNP delivery efficiency by mediating cell uptake and endosomal escape [28,29]. Furthermore, LNP internal charge interactions, as well as the surface charge, direct the delivery of LNPs to different tissues following systemic administration [26]. Thus, evaluating how LNP chemical makeup impacts mRNA delivery is required to develop a platform for preferential accumulation in the placenta. Toward this goal, we conducted a Design of Experiments (DOE) study to systematically investigate how LNP composition influences mRNA delivery to the placenta.

The importance of developing LNPs for placenta-specific therapy is multi-fold [30–32]. Placental dysfunction is responsible for severe obstetric complications, such as preeclampsia, Hemolysis, Elevated Liver enzymes, Low Platelet count (HELLP) syndrome, and fetal growth restriction [33–35]. The only curative treatment option for some of these, such as severe preeclampsia, is to induce preterm delivery, which may have detrimental impacts on fetal development and survival depending on the stage of gestation [36,37]. Although a complete mechanistic understanding of the pathologies behind preeclampsia and fetal growth restriction remains unknown, several investigations have shown elevated levels of circulating soluble fms-like tyrosine kinase-1 (sFlt-1) and decreased levels of placental growth factor (PlGF) in the blood of pregnant individuals with these conditions [38–41]. PlGF contributes to proangiogenic signaling in the placenta by binding vascular endothelial growth factor receptor 1 (VEGFR-1) on endothelial cells [42]. sFlt-1 binds and inactivates PlGF in the circulation, resulting in reduced VEGFR-1 signaling and endothelial dysfunction [42]. A high ratio of sFlt-1:PlGF compared to healthy pregnancy has been proven useful in predicting the development of early-onset preeclampsia and fetal growth restriction [34,39,41,43–45]. Due to its potential as a therapeutic target in placenta-related diseases [46,47], here we deliver PlGF mRNA in LNPs as a model for protein replacement therapy.

Through a DOE approach, we have developed a library of LNPs to investigate how LNP composition impacts mRNA delivery to trophoblasts and the placenta to identify a top formulation with the potential to treat placenta-related diseases. Our *in vitro* screen revealed that the combination of the widely studied ionizable lipid, C12-200, with 1,2-dioleoyl-*sn*-glycero-3-phosphoethanolamine (DOPE) phospholipid, is required for potent mRNA delivery to trophoblasts. In further evaluating LNPs prepared with both C12-200 and DOPE, we found a linear correlation between the amount of PEG and the apparent pKa of LNPs. Reducing the PEG molar amount resulted in higher apparent pKa, which may drive delivery to trophoblasts *in vitro*. We also identified LNP formulations that have high delivery of luciferase or PlGF mRNA in mouse placentas with no delivery to the fetuses. Together, our results provide the foundation of an LNP platform that delivers therapeutic mRNA to the placenta as a potential treatment for diseases originating from placental dysfunction.

2. Results and discussion

LNP Library Formulation and Characterization. A definitive screening design (DSD) was used to create a library of 18 chemically unique LNPs (A1-A18) from the design space available, as previously described [24,48–50]. A DSD is a DOE approach commonly used for early-stage experimentation involving a combination of three-level continuous and two-level categorical factors to identify linear and quadratic effects [48,49]. Here, we used LNP formulation parameters as factors in the DSD. We defined two categorical factors - type of ionizable lipid and type of phospholipid - and three continuous factors - molar percentages of ionizable lipid, phospholipid, and (1,2-dimyristoyl-*sn*-glycero-3-phosphoethanolamine-*N*-[methoxy (polyethylene glycol)-2000] (ammonium salt)) (DMPE-PEG). We used two established ionizable lipids, C12-200 or DLin-MC3-DMA, to assess how ionizable lipid structure impacts delivery to trophoblasts. C12-200 has been evaluated in LNPs for both siRNA and mRNA delivery in a variety of cell types and animal models [24,25,29,51–53]. DLin-MC3-DMA is the ionizable lipid in the FDA-approved therapy to treat hereditary transthyretin-mediated amyloidosis [13,14]. We also compared LNP delivery using two phospholipids, 1,2 distearoyl-*sn*-glycero-3-phosphocholine (DSPC) or 1,2-dioleoyl-*sn*-glycero-3-phosphoethanolamine (DOPE) (Fig. 1A, Fig. S1). We varied the molar percentages of ionizable lipid (25–45 %), phospholipid (10–22 %), and DMPE- PEG (1.5–3.5 %) used to make LNPs based on prior literature [24,52] (Fig. 1B, Table S1). The remaining molar composition (to add up to 100 %) for each LNP was cholesterol. This design choice was based on prior literature showing that the types and amounts of ionizable lipid, phospholipid, and PEG influence hepatocellular mRNA delivery [19,24,28,29,51]. Thus, we included these as factors in our DSD to investigate their effect on trophoblast mRNA delivery, and the amount of cholesterol in each formulation was calculated as the remainder of each recipe. Since the DSD did not include cholesterol as an independent factor, it could not be included in the statistical analysis. In initial studies, we encapsulated luciferase mRNA into LNPs as it is detectable and quantifiable using a plate reader for *in vitro* experiments and via an In Vivo Imaging System (IVIS) for *in vivo* studies.

The hydrodynamic diameters of LNPs in the library ranged from 92.4 to 164.0 nm (Fig. 2A, Table S1-1.1) and the polydispersity indices (PDI) ranged from 0.120 to 0.317 (Fig. 2B, Table S1-1.1). The zeta potential of LNPs in the library ranged from −8.52 to 19.45 mV (Fig. 2C, Table S1). To track LNP stability over time, we measured the hydrodynamic diameter and PDI of LNPs 50 and 100 days following formulation (Table S1.2). LNPs were stored at 4 °C for the duration of the experiment. The PDI of some LNPs increased over time while in storage, ranging from 0.170 to 0.586 (Table S1.2). This may indicate a less monodisperse solution over the 100 day test period, which could result from LNP aggregation or degradation [54]. We also characterized the mRNA encapsulation efficiency, which ranged from 35.6 % to 83.2 % encapsulation relative to the amount of mRNA added during formulation (Fig. 2D, Table S1-1.1). To evaluate encapsulation stability over time, the encapsulation efficiency was calculated one month post-formulation for select LNPs. We found that the encapsulation efficiencies for LNPs A5, A8, A10, and A14 decreased <20 % over one month, while the encapsulation efficiency for LNP A3 decreased 28 %. Together, these results indicate that encapsulation is stable over one month, but future studies would need to be conducted to evaluate longer timepoints.

The surface ionization was evaluated by a 6-(*p*-toluidinyl)naphthalene-2-sulfonic acid (TNS) assay and reported as the apparent pKa (Fig. 2E, Table S1), ranging from 5.298 to 7.111. Apparent pKa measured in this way represents the pH at which half of the ionizable

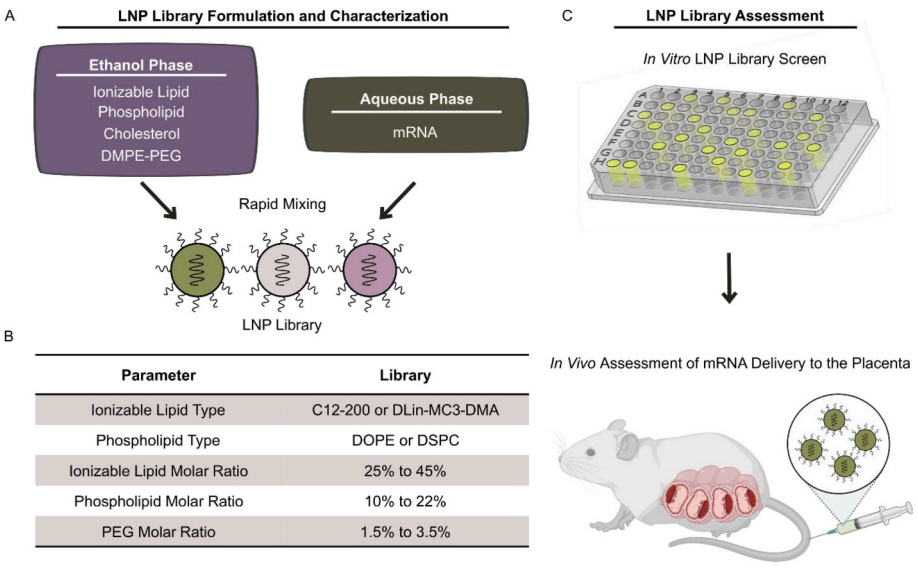

Parameter	Library
Ionizable Lipid Type	C12-200 or DLin-MC3-DMA
Phospholipid Type	DOPE or DSPC
Ionizable Lipid Molar Ratio	25% to 45%
Phospholipid Molar Ratio	10% to 22%
PEG Molar Ratio	1.5% to 3.5%

Fig. 1. (A) LNPs are formulated by rapidly mixing lipid components in an ethanol phase and mRNA in an aqueous phase consisting of pH 3 citrate buffer. (B) Ranges of parameters used in the DSD to make the library (A1-A18). (C) The library was assessed *in vitro* with encapsulated luciferase mRNA and *in vivo* with encapsulated luciferase or PlGF mRNA.

lipids are protonated to induce endosomal escape and cytoplasmic mRNA delivery [29,53]. We utilized a DSD fit analysis to identify which LNP formulation parameters, defined as factors in the DSD, influence apparent pKa as main effects or pairwise interactions (refer to the Materials and Methods section for full details on the analysis). Through this analysis, a main effect is defined as the effect of a single LNP formulation parameter on the apparent pKa, and a pairwise interaction is the combined effect of two LNP formulation parameters on the apparent pKa. We found that the type of ionizable lipid was a main effect for apparent pKa ($p < 0.001$, Fig. S2) with C12-200 in LNPs yielding lower apparent pKa values compared to DLin-MC3-DMA (Table S1). The 18 LNPs formulated through our DSD were used to assess luciferase mRNA delivery *in vitro* and *in vivo*, as described below.

LNP Composition Dictates Delivery to Trophoblasts. To assess how LNP composition impacts delivery *in vitro*, we treated BeWo b30 trophoblast cells (referred to as BeWos hereafter) with each LNP at 0 or 100 ng/well for 24 h. LNP A10 yielded ~190,000-fold higher luciferase expression compared to phosphate-buffered saline (PBS)-treated cells ($p < 0.0001$, Fig. 2F, Table S2, S2.1). LNPs A5, A8, and A14 had the next highest luciferase expression compared to PBS-treated cells ($p < 0.001$, Fig. 2F). Interestingly, these four top-performing LNPs were comprised of C12-200 and DOPE as the ionizable lipid and phospholipid, respectively (Fig. 2G). No LNPs prepared with DLin-MC3-DMA or DSPC yielded high luciferase expression (Fig. 2G), beyond 45,000-fold above the PBS-treated cells. This importance in ionizable lipid choice aligns with prior work that demonstrated that the ionizable lipid structure, and in particular the polyamine headgroup, drives delivery efficiency [17]. Based on our results demonstrating LNPs with C12-200 and DOPE yielded the highest mRNA delivery (Fig. 2G), we assessed all five LNPs from Library A containing both C12-200 and DOPE - LNPs A3, A5, A8, A10, and A14. Following a dose-response experiment in BeWos, these five LNPs showed large differences in luminescence despite containing the same lipids (Fig. 2H). Similar to the initial screen, LNP A10 and LNP A3 had the highest and lowest expression of these five LNPs, respectively, at all doses (Fig. 2H, Table S3). In addition to luciferase expression, we assessed BeWo viability following LNP treatment using MTT (3-(4,5-dimethylthiazol-2-yl)-2,5-diphenyltetrazolium bromide) tetrazolium reduction assays (referred to as MTT hereafter). Only cells treated with LNPs A6 ($p = 0.011$) and A11 ($p = 0.023$) had reduced viability compared to the PBS-treated cells (Fig. 2F, Table S4-4.1), indicating that the majority of LNP formulations are not toxic to BeWos.

We analyzed the DSD to determine the important LNP parameters affecting viability of BeWos. This demonstrated that the type of ionizable lipid ($p = 0.005$), type of phospholipid ($p = 0.018$), ionizable lipid amount ($p < 0.0001$), and phospholipid amount ($p = 0.016$) were significant factors (Fig. S3). The two LNPs that resulted in significantly lower viability compared to the controls were comprised of low amounts of DLin-MC3-DMA and DOPE – 25 % and 10 %, respectively – which was confirmed by our DSD analysis. Additionally, the model found pairwise interactions between type of phospholipid and phospholipid amount ($p < 0.0001$), and type of phospholipid and ionizable lipid amount ($p < 0.0001$, Fig. S3).

Next, we evaluated the DSD for factors affecting transfection. We found that the type of ionizable lipid ($p = 0.018$) and type of phospholipid ($p = 0.017$) were signficant factors affecting transfection (Fig. S4), with C12-200 or DOPE in LNPs yielding the strongest luciferase expression overall compared to the other LNP lipid components. Additionally, the model found several pairwise interactions between the type of ionizable lipid and PEG amount ($p = 0.036$), type of phospholipid and PEG amount ($p = 0.034$), and type of ionizable lipid and type of phospholipid ($p = 0.0105$, Fig. S4). This indicates that the mechanism by which each LNP parameter affects LNP transfection is more complicated than an additive manner of main effects, as it involves several pairwise interactions. Based on this, it is pertinent to study both the main effects and pairwise interactions when researchers are developing LNPs for nucleic acid delivery. In particular, the pairwise interactions revealed that maximal delivery occurs when C12-200 and DOPE are both included in the LNP formulation ($p = 0.0105$, Fig. S4). This finding agrees with prior literature comparing mRNA delivery with LNPs made with DOPE or DSPC, as the use of DOPE was found to yield higher transfection than LNPs made with DSPC [24,52]. A limitation of DSDs to build a LNP library is the possibility of other high-performing LNPs potentially missed within the design space. Although it is not feasible to test every LNP formulation (as there are thousands of possible combinations), our data shows that C12-200 and DOPE are the key drivers for mRNA delivery to trophoblasts.

To consider the influence of hydrodynamic diameter on mRNA delivery, we fit the hydrodynamic diameter versus luciferase expression with a linear regression, which had an R^2 coefficient of determination of 0.023 (Fig. 3A). This indicates that there is not a linear relationship between hydrodynamic diameter and luciferase expression, suggesting that LNP size does not signficantly influence LNP delivery. To further

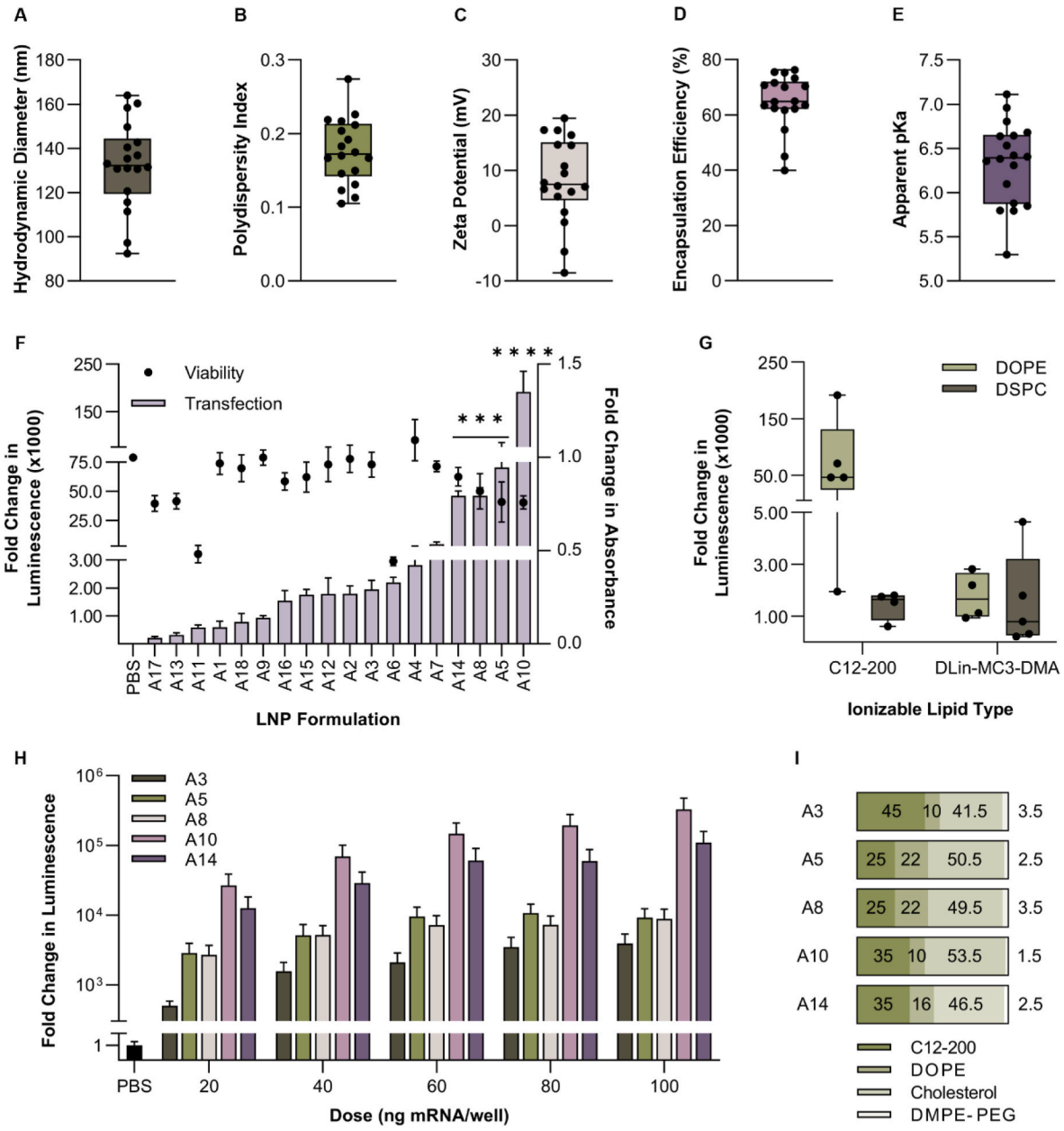

Fig. 2. (A) Hydrodynamic diameter intensity, (B) polydispersity index, (C) zeta potential, (D) encapsulation efficiency, and (E) apparent pKa of LNPs in the library. Each dot represents an individual LNP from the library. (F) Luminescence from BeWos treated with LNPs A1-A18 was calculated as a fold change over the PBS-treated group (left axis), and viability is represented as a fold change in absorbance over the PBS-treated group following the MTT assay (right axis). Data reported as fold change and standard error of the mean (n = 6). (G) Luminescence from BeWos following treatment with LNPs A1-A18 grouped by type of ionizable lipid and phospholipid. Each dot represents an individual LNP from the library. (H) Fold change in luminescence following treatment with LNPs at dosages ranging from 0 to 100 ng mRNA/well, reported as the mean and standard error of the mean. (I) Molar ratios of the five LNPs containing C12-200 and DOPE that were used in further studies. ***$p < 0.001$ and ****$p < 0.0001$ compared to the PBS-treated cells analyzed by a Kruskal-Wallis test.

confirm that size does not drive delivery, we grouped LNPs into three size categories – <120 nm, 130–139 nm, >140 nm – and compared the delivery efficiency, finding no signficant difference in delivery (Fig. S5). Therefore, we hypothesized that variance in luciferase expression is due to differences in the molar ratios of each lipid component within the LNPs affecting the apparent pKa [55]. For example, LNP A10 is comprised of C12-200:DOPE:Cholesterol:PEG molar ratios of 35:10:53.5:1.5 and has an apparent pKa of 6.308; by comparison, LNP A14 is comprised of the molar ratios 35:16:46.5:2.5 and has an apparent pKa of 5.848 (Fig. 2I, Table S1). To explore which LNP component is driving the differences in delivery, we plotted the apparent pKa versus the PEG and DOPE molar ratio for LNPs A3, A5, A8, A10, and A14 and observed that LNPs containing a lower PEG molar ratio had a higher apparent pKa (Fig. S6D, Table S6). Comparatively, there was no relationship between the DOPE, cholesterol, or C12-200 molar ratios and apparent pKa (Figs. S6A–C, Table S5).

To further investigate how PEG and DOPE molar ratios impact delivery, we prepared three new LNPs in addition to the original A10 and A14 formulations. These new formulations contained the lower, center, and higher molar ratios of PEG and DOPE from LNPs A10 and A14 (Fig. 3B, Table S6). We explored the differences in PEG and DOPE molar ratios because A10 and A14 have similar formulation parameters – both contain 35 % C12-200 – but show large differences in luciferase expression *in vitro* (Fig. 2F, H). The hydrodynamic diameter,

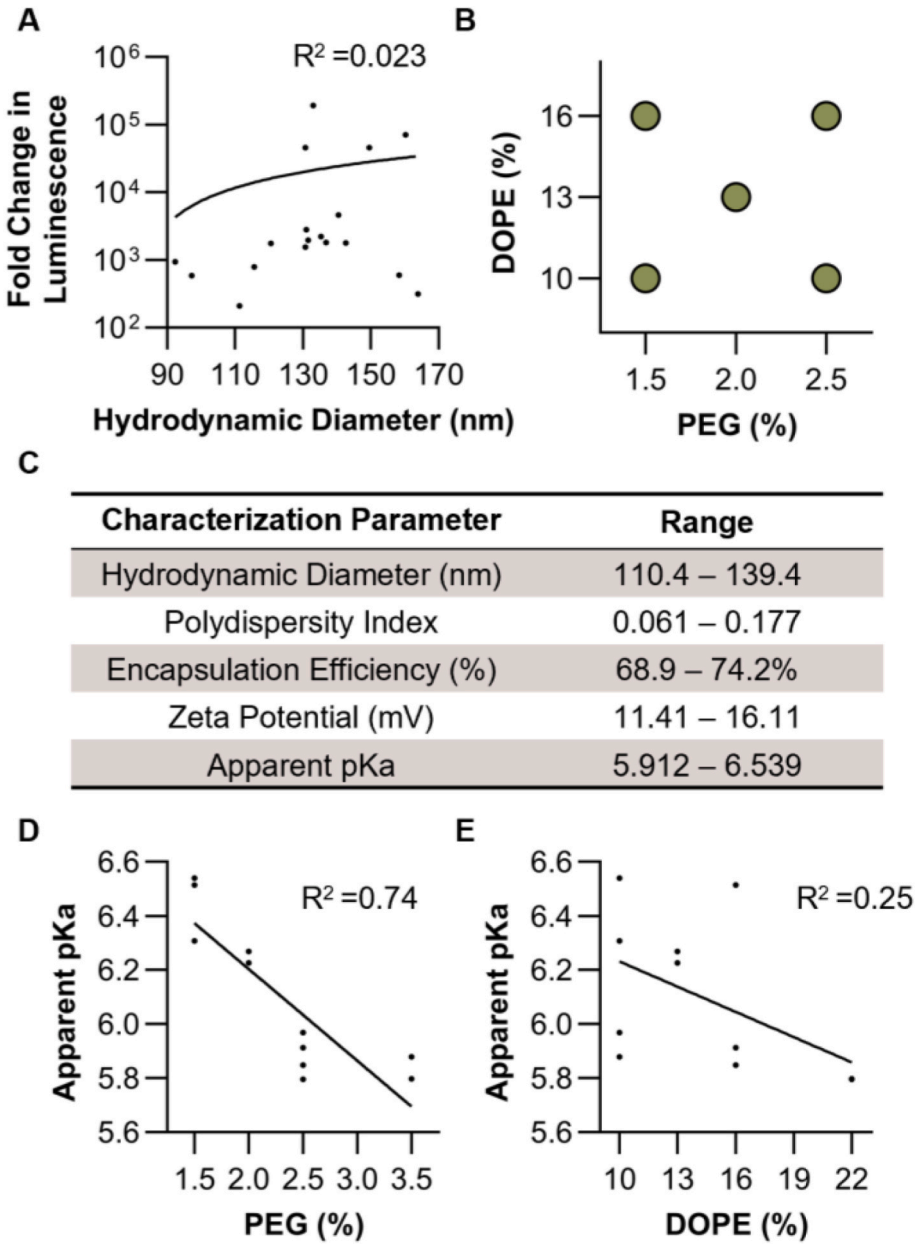

Fig. 3. (A) Fold change in luminescence plotted against hydrodynamic diameter (B) Six LNPs (two center points) were formulated with 10, 13, or 16 % DOPE and 1.5, 2.0, or 2.5 % PEG. (C) Characterization of the six LNPs. (D) Apparent pKa of the six LNPs and C12-200/DOPE LNPs from Library A (A3, A5, A8, A10, A14) plotted against the PEG molar ratio in the LNP formulation. (E) Apparent pKa of LNPs plotted against the DOPE molar ratio. R^2 coefficient of determination values calculated by linear regression analysis.

polydispersity index, mRNA encapsulation efficiency, zeta potential, and apparent pKa were measured for these new LNPs (Fig. 3C, Table S6). We plotted the apparent pKa of the new LNPs and Library A LNPs that contained C12-200 and DOPE (LNPs A3, A5, A8, A10, and A14) versus the PEG (Fig. 3D) and DOPE molar ratios (Fig. 3E). The data was fit with a linear regression with R^2 coefficients of determination of 0.736 for apparent pKa versus PEG and 0.247 for apparent pKa versus DOPE (Fig. 3D and E, Table S7). The linear relationship between apparent pKa and PEG molar ratio indicates that a lower PEG molar ratio results in a higher apparent pKa. Here, a PEG molar ratio of 1.5 % resulted in an apparent pKa between 6.3 and 6.5. Our LNP with the highest mRNA delivery in BeWos, LNP A10, contained 1.5 % PEG and had an apparent pKa of 6.308. The pKa of LNP A10 aligns well with prior literature demonstrating that pKa values between 6.0 and 6.5 may be ideal for *in vivo* siRNA delivery [28,29,53]. LNPs A3, A5, A8, and A14 had higher PEG molar ratios of 3.5 %, 2.5 %, 3.5 %, and 2.5 % and lower apparent pKa's of 5.878, 5.795, 5.798, and 5.848, respectively. The lower apparent pKa values of these LNPs, compared to A10, indicate a less protonated LNP surface, which can decrease cellular uptake and endosomal escape, as demonstrated by the *in vitro* data (Fig. 2F, H) [56].

Based on the *in vitro* delivery results and the low toxicity of these LNPs, we selected LNPs A3, A14, and A10 as low, medium, and high-performing LNPs for further studies in the remainder of this work. Importantly, LNPs A3, A14, and A10 also exhibited similar encapsulation efficiencies (61.75–63.35 %) and hydrodynamic diameters (130.8–133.0 nm) (Table S1), allowing us to directly compare their delivery efficiency based on their lipid compositions.

LNPs Deliver mRNA to Placentas Following IV Administration. We injected pregnant CD1 mice (dams) at embryonic day (E) 17.5 with LNPs A3, A10, and A14 via the tail vein (0.5 mg mRNA/kg body weight).

After 4 h, we imaged the dam, placentas, fetuses, and maternal organs sequentially by IVIS (Fig. 4A). LNP A14 yielded the highest luminescence in the dam organs overall compared to dams treated with LNPs A3 and A10 (Fig. 4A and B, Table S8). The liver and spleen had the highest and second highest luciferase expression, respectively, compared to all other dam organs, for all LNPs. This high level of liver and spleen delivery agrees with prior literature due to high blood flow to these tissues and apolipoprotein E-mediated uptake [57,58].

Next, we imaged the placentas and fetuses collected from saline- or LNP-treated dams. Importantly, no LNPs resulted in detectable luciferase expression in the fetuses by IVIS (Fig. 4A). A nested mixed effects model revealed that LNP A14 had significantly higher luciferase expression in the placentas overall compared to LNPs A3 ($p = 0.031$) and A10 ($p = 0.042$) and the saline group ($p = 0.026$, Fig. 4C Table S8.1). Of note, LNP A14 is the same formulation that was previously designed for high mRNA delivery to mouse livers [24]. Thus, LNP A14 was expected to have the best delivery efficiency in the liver, which may be attributed to its less protonated surface (apparent pKa of 5.848) [24,56]. However, the luciferase expression in the placenta following LNP A14 delivery contradicted our *in vitro* results that showed LNP A10 yielded significantly higher mRNA delivery in trophoblasts (Fig. 2F). As described above, the high luciferase expression from LNP A10 *in vitro* is due to a lower molar amount of PEG in the LNP formulation causing an increase in apparent pKa compared to LNP A14 (Fig. 3D). This same logic does not apply to an *in vivo* model, as studies have shown that PEG-lipids are desorbed from LNPs within 2 h following systemic administration [59]. This indicates that the amount of PEG may not influence delivery to the placenta *in vivo*. Thus, our findings correlating PEG molar ratio to apparent pKa appear to be relevant for *in vitro* delivery more so than *in vivo* systemic delivery. LNP delivery results to cells *in vitro* often do not correlate with delivery efficiency *in vivo*. [60,61] This limitation can be lessened by using primary human or mouse cells, rather than cell lines, and consistent LNP formulation techniques to improve *in vitro* and *in vivo* delivery correlation [61]. Furthermore, the use of DOEs, such as the approach herein, and iterative library design allows for the collection of more *in vitro* data to predict which factors in the LNPs will have signficant effects on *in vivo* efficacy.

We sought to further elucidate the applicability of LNPs for mRNA delivery to the placenta. We directly compared luciferase expression in the liver and spleen to the placentas by calculating liver:placenta (L:P) and spleen:placenta (S:P) delivery ratios using the average radiance with background subtracted for each image. The L:P ratio was 1.9-fold lower, and the S:P ratio was 4.9-fold lower, in mice treated with LNP A10 compared to those treated with LNP A14 (Fig. 4D). While not statstically significant, this may indicate that LNP A10 is more efficient at delivering mRNA to the placenta relative to the liver and spleen compared to LNP A14. Thus, LNP A10 may be bias towards placental delivery, which may limit off-target effects when treating placental dysfunction.

LNP-Mediated Delivery of PlGF mRNA. Next, we evaluated placental delivery of these platforms using PlGF mRNA as a more therapeutically-relevant mRNA to demonstrate induced protein synthesis and secretion from the placenta. As explained above, circulating PlGF levels are decreased in diseases of pregnancy, such as preeclampsia and fetal growth restriction, compared to a healthy pregnancy [41,44]. The reduced PlGF increases the sFlt 1:PlGF ratio, contributing to decreased angiogenesis in the placenta that is found in preeclampsia [39,41,62]. Thus, we formulated LNPs with PlGF mRNA with the goal of increasing circulating PlGF and local PlGF expression in the placenta. The remainder of our data herein uses LNPs with encapsulated PlGF mRNA in place of the luciferase mRNA used in prior studies. We treated BeWos with LNPs A3, A10, or A14 and assessed secreted PlGF content after 24 h. At most doses, BeWos treated with LNP A10 produced the highest PlGF levels compared to the other formulations and free mRNA (Fig. 5A, Table S9). LNP A10 yielded 1.58-fold higher PlGF secretion compared to LNP A14 at a dose of 200 ng mRNA/well. This agrees with our *in vitro* results with luciferase mRNA (Fig. 2F–H), as it demonstrates that LNP A10 is the most efficient at delivering mRNA to BeWos *in vitro*.

We also assessed PlGF mRNA delivery *in vivo*. LNPs A3, A10, and A14 were injected via the tail vein (0.5 mg mRNA/kg body weight) (Fig. 5B). For these studies, we analyzed PlGF content in dam serum after 4 and 24 h to track the secretion kinetics of PlGF over time. At 4 h after injection, LNP A3 produced 111.4 ng/mL PlGF in the dam serum, compared to 103.6 and 46.6 ng/mL of PlGF produced following treatment with LNPs A10 and A14, respectively (Fig. 5C, Table S10). Treatment with A3 ($p = 0.0219$) and A10 ($p = 0.0069$) had a statstically signficant increase in PlGF in the serum compared to free mRNA at 4 h (Fig. 5C, Table S10.1).

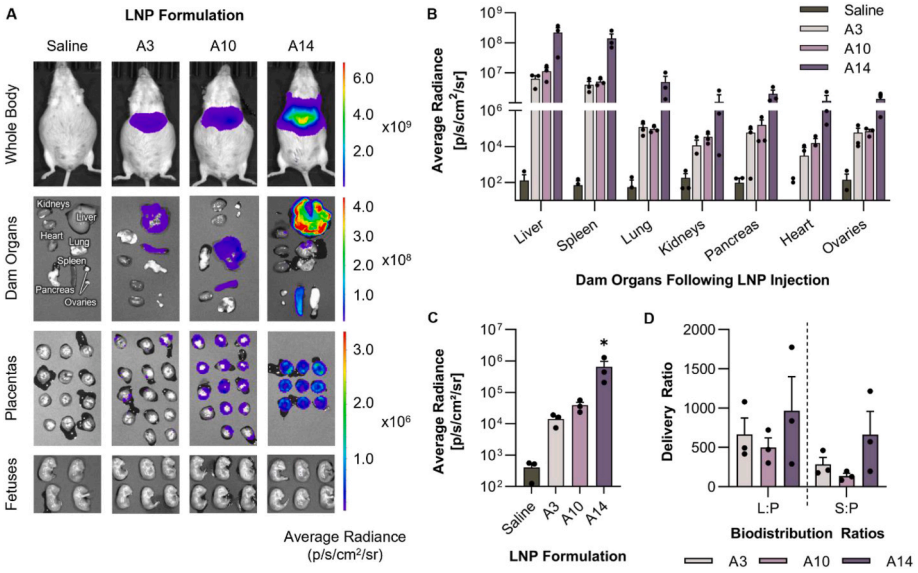

Fig. 4. (A) IVIS images of dams, maternal organs, placentas, and fetuses 4 h after treatment with saline or LNPs A3, A10, or A14. Fetal images contain a representative group of fetuses from that treatment group, selected randomly. (B) Quantification of normalized radiance with background subtracted for each maternal organ (n = 3). (C) Quantification of normalized radiance with background subtracted for all the placentas from each dam 4 h after treatment. Each marker (n = 3) represents the average of all placentas in one dam. (D) Liver to placenta (L:P) and spleen to placenta (S:P) delivery ratios for dams treated with LNPs A3, A10, and A14 (n = 3). All bar graphs report the mean and standard error of the mean for the treatment group. *$p < 0.05$ compared to the saline-treated cells analyzed by a nested mixed effects model.

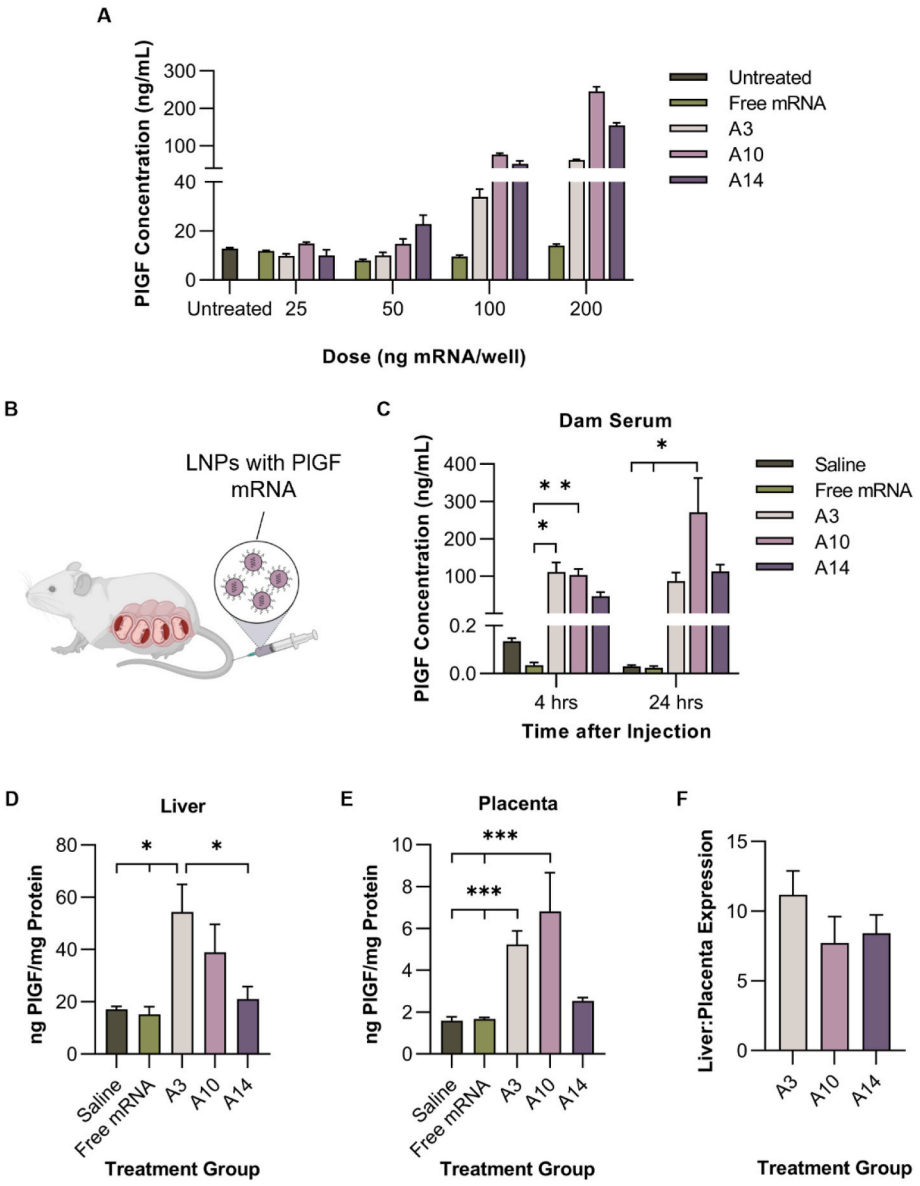

Fig. 5. (A) PlGF concentration from supernatant of BeWos treated with LNPs at varying doses. (B) In the remainder of this work, dams were treated with LNPs encapsulated with PlGF mRNA as a model for a secreted therapeutic protein. (C) PlGF levels in dam serum collected 4 and 24 h following injection with saline, free mRNA, or LNPs A3, A10, or A14 (n = 4). PlGF expression in the (D) dam livers (n = 4) and (E) placentas (n = 8, 1 placenta from the left and 1 placenta from the right side of the uterine horn per dam). (F) Ratio of PlGF expression in the liver compared to the placenta (n = 4). All bar graphs report the mean and standard error of the mean for each treatment group. *$p < 0.05$ and ***$p < 0.001$ compared to the PBS-treated cells or saline-treated dams analyzed by Kruskal-Wallis (serum and placentas) and Ordinary One-Way ANOVA (livers) tests.

At 24 h, LNP A10 produced 270.2 ng/mL of PlGF in the dam serum compared to 86.6 and 113.4 ng/mL of PlGF produced following treatment with LNPs A3 and A14, respectively (Fig. 5C, Table S10). Treatment with LNP A10 yielded a statistically significant increase in PlGF in the serum compared to dams treated with saline ($p = 0.019$) and free mRNA at 24 h ($p = 0.013$, Fig. 5C, Table S10.2). The difference between serum concentration of PlGF at 4 and 24 h was compared for each treatment group by a Wilcoxon test (Table S10.5). None of the treatment groups produced a statistically different amount of PlGF at 24 h compared to 4 h. However, it is noteworthy that LNP A10 yielded approximately 2.5× higher PlGF at 24 h compared to 4 h ($p = 0.125$). Although not statistically significant, these data indicate that the LNP formulation may impact how quickly the mRNA is delivered and secreted from the placenta. Overall, our data does not demonstrate significant degradation or clearance of PlGF 24 h after LNP delivery.

Although our data demonstrates that LNP A10 yields the highest level of PlGF secretion in dam serum, we next sought to explore which tissues were generating the secreted PlGF. Since our overall goal is to develop an LNP platform for placental delivery, we examined the level of PlGF generated in the placenta and liver tissues. We compared PlGF levels in the liver because our prior data (Fig. 4A and B) demonstrated a high level of liver delivery. Dams treated with LNP A3 had the highest liver PlGF content with 54.4 ng of PlGF/mg of total protein ($p < 0.05$, Fig. 5D, Table S10.3). Alternatively, dams treated with LNP A10 had the highest PlGF content in the placenta with 6.81 ng PlGF per mg of total protein, which is 1.30-fold and 2.69-fold higher than LNPs A3 and A14, respectively ($p < 0.001$, Fig. 5E, Table S10.4). These results are consistent with *in vitro* results using PlGF mRNA, where LNP A10 had the highest PlGF secretion from BeWos (Fig. 5A). This data contradicts our studies with luciferase mRNA at the time points studied, which found that LNP A14 yielded highest delivery overall *in vivo* compared to the other LNP formulations. This indicates that, in addition to LNP design,

the mRNA sequence also plays a critical role for *in vivo* biodistribution.

A delivery ratio comparing PlGF levels in the liver to PlGF levels in the placenta demonstrated that LNP A10 exhibited the lowest liver: placenta (L:P) ratio that was 1.45-fold and 1.09-fold lower than LNPs A3 and A14, respectively (Fig. 5F). This result, combined with the higher serum PlGF content, indicates that LNP A10 is more efficient at delivering PlGF mRNA to the placenta compared to LNPs A3 and A14. Local placental delivery is important because PlGF levels in the placenta promote endothelial growth, vasculogenesis, and overall placental development [63]. Recent evidence suggests the role of PlGF on endothelial-dependent relaxation mechanisms [64], which may be advantageous locally in the placenta to improve uterine and placental vessel remodeling, while increasing blood flow to the fetus. Moving forward, we aim to incorporate targeting ligands into this platform to further increase local placental delivery. Based on the data presented here, we have developed an LNP platform (A10) that delivers multiple types of mRNA to the placenta.

Toxicity Analysis. Lastly, we assessed toxicity of the LNPs with

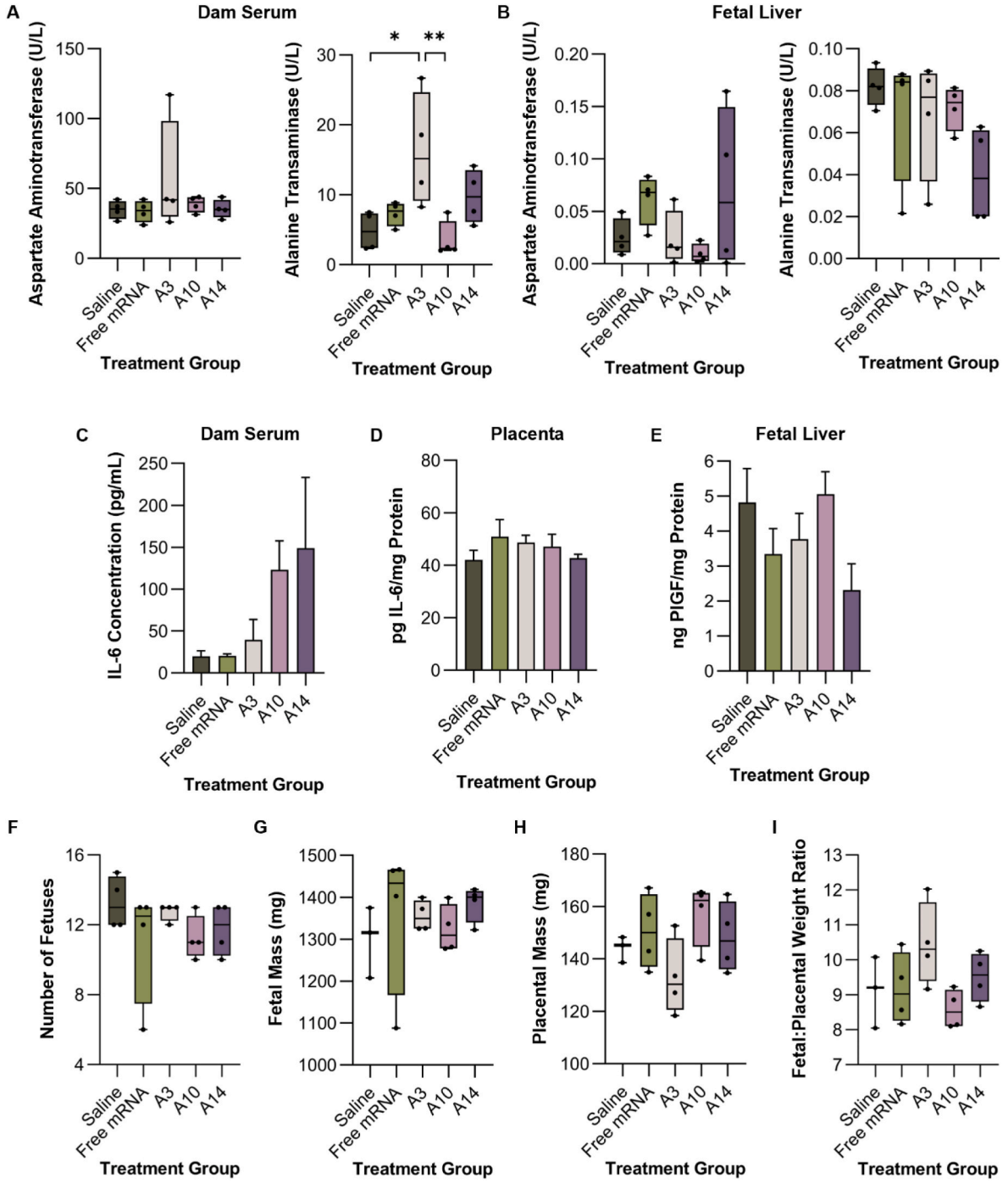

Fig. 6. AST and ALT levels in (A) dam serum and (B) fetal liver tissue 24 h after treatment with LNPs encapsulating PlGF mRNA (n = 4). IL-6 levels in (C) dam serum (n = 3) and (D) placenta tissue (n = 4). (E) PlGF content in fetal liver tissue (n = 4). Bar graphs report the mean and standard error of the mean for each treatment group (F) Number of fetuses averaged for each dam (n = 4) with each treatment group 24 h after treatment at the time of extraction. (G) Fetal mass and (H) placental mass averaged for all the fetuses from each dam (n = 4) within each treatment group at the time of extraction. (I) Ratio of fetal to placental mass averaged for each dam (n = 4). *p < 0.05 and **p < 0.01 compared to the saline-treated dams analyzed by Ordinary One-Way ANOVA and Kruskal-Wallis tests.

encapsulated PlGF mRNA to both the dams and fetuses. Serum from dams treated with LNPs A3, A10, and A14 was examined for aspartate aminotransferase (AST) and alanine transaminase (ALT) content to assess liver toxicity, which yielded no significant difference between AST levels in dam serum from all treatment groups (Fig. 6A). The only significant difference in serum ALT levels was from dams treated with LNP A3 compared to both saline ($p = 0.017$) and LNP A10 ($p = 0.008$, Fig. 6A, Table S11–11.2). These results indicate that LNP A10, our top-performing LNP for PlGF delivery *in vivo*, does not yield liver damage as assessed by enzyme release in dams. We also assessed AST and ALT content in fetal liver tissues following treatment, which revealed no significant differences between fetuses from dams treated with each treatment group. Interestingly, two fetuses taken from dams treated with LNP A14 had slightly elevated AST (0.007 compared to 0.134 U/mg of total protein) that was not statistically significant (Fig. 6B, Table S11.3-11.4).

We measured concentration of interleukin-6 (IL-6) in dam serum and placenta tissues 24 h after treatment to investigate the acute inflammatory response to LNPs [65]. LNPs have been evaluated as adjuvants for vaccines because they induce IL-6 production [65,66]. IL-6 concentration in the dam serum was elevated following delivery of LNPs, compared to saline and free mRNA, but statistical analysis showed no significance between groups (Fig. 6C, Table S11.5). Additionally, serum concentrations of IL-6 were below levels seen in previous studies of mice treated with LNPs containing mRNA [65–67]. We also examined local inflammation in the placenta by measuring IL-6 concentration in digested placenta tissues, which yielded no differences between groups (Fig. 6D, Table S11.6). This indicates that any changes in systemic IL-6 production do not originate from local immune activation in the placenta.

To evaluate potential fetal delivery of LNPs, we measured PlGF content in the digested fetal liver tissues (Fig. 6E). There was no significant difference between PlGF expression in the fetal livers from dams treated with LNPs compared to dams treated with saline, indicating no delivery to the fetus (Table S12–12.1). As another measure for toxicity, we averaged the number of fetuses per dam at the time of dissection and tissue collection, which showed no significant difference between number of fetuses from all treatment groups (Fig. 6F, Table S13–13.1). For this study, we determined viability based on fetal size as well as no visible tissue resorption. Any fetuses that were obviously resorbed were considered non-viable and were not included in any analysis. The fetuses and their respective placentas from each dam were weighed at the time of tissue collection, which revealed no difference between treatment groups (Fig. 6G and H, Table S13.2-13.3). Using this data, we calculated a fetal to placental (F:P) weight ratio for each fetus and its placenta, which indicates the overall health of the fetus and placenta with no difference between treatment groups (Fig. 6I, Table S13.4) [68–70]. Taken together, our toxicity analyses indicate that our top platform, LNP A10, is nontoxic to both the dams and the fetuses following treatment. These results, combined with the high luciferase and PlGF mRNA delivery, demonstrate that LNP A10 may serve as a potent and safe drug delivery platform for placenta-related diseases.

Research on placenta-related diseases has identified low PlGF as a clinical biomarker of preeclampsia and fetal growth restriction. However, limited studies have investigated PlGF as a protein replacement therapy to restore angiogenic factor balance for these diseases [71–73]. In mouse models of preeclampsia, intraperitoneal injection with recombinant mouse or human PlGF decreased arterial blood pressure and circulating sFlt-1 [71,72]. Subcutaneous injection with recombinant human PlGF into nonhuman primates with surgically induced uteroplacental ischemia decreased blood pressure, proteinuria, and sFlt-1 mRNA expression in the placenta [73]. These studies show that increased circulating PlGF improved clinical outcomes in animal models of preeclampsia [71–73], validating its potential use as a therapeutic.

Normal serum levels of PlGF in humans varies based on gestational age, peaking around 30 weeks in the third trimester. Below a serum PlGF level cutoff between 80 and 120 pg/mL is considered predictive of adverse pregnancy outcomes [44]. Patients with low serum PlGF levels (<100 pg/mL) at the time of testing (20–35 weeks of gestation) were 58.2 % more likely to develop early-onset preeclampsia (<34 weeks of gestation) [74,75]. Our results demonstrate that LNPs have the potential to produce PlGF secretion *in vivo* at levels much greater than what is seen in human pregnancy. Our top formulation, LNP A10, yielded approximately two orders of magnitude higher PlGF levels in the dam serum compared to what is typically seen during pregnancy (~160–1800 pg/mL) [40]. This indicates that further studies regarding the dosing would be warranted to potentially lower the administered dose to achieve normal levels. However, it is important to note that the physiological differences between mouse and human pregnancy would likely contribute to the level of PlGF secretion observed. For example, mice in our studies carried up to 15 fetuses in a pregnancy, whereas the majority of human pregnancies have one fetus and placenta. Thus, the high level of PlGF secretion may be a result of multiple placentas secreting PlGF. Directly corresponding our results to human pregnancy will require further studies in larger animal models, such as sheep or non-human primates. In the future, we aim to use our top LNP formulations in preeclamptic animal models to assess the impact of PlGF mRNA delivery in placenta pathology and function.

There are a few off-target effects of administering PlGF that should be considered. For example, constitutively expressed PlGF in a transgenic mouse model yielded enhanced vessel permeability [76] and inhibition of apoptosis [77]. The LNP platform described herein overcomes these off-target effects because protein expression following mRNA delivery is transient. The short half-life of mRNA is a major benefit of this platform during pregnancy. The goal of disease management during pregnancy, as described here, is to extend pregnancy several weeks to reduce the risks of preterm birth. Since the goal is not permanent gene therapy, many of the long-term risks associated with PlGF administration are alleviated. Although the LNPs described here, similar to other nanoparticle delivery systems, yield liver delivery, our top LNP A10 resulted in the lowest liver:placenta ratio compared to the other formulations tested. In the future, we will incorporate targeting ligands into LNPs to improve placental targeting and minimize off-target effects to maternal tissues. Finally, our biodistribution results using luciferase mRNA encapsulated in LNPs demonstrated no delivery of LNPs to the fetus. This, combined with our toxicity analysis, suggests no adverse effects of LNPs to fetuses. These results support the use of LNPs, and in particular, LNP A10, for mRNA delivery to the placenta to treat diseases that originate from placental dysfunction.

3. Conclusions

This investigation utilized a DSD to identify LNPs for effective mRNA delivery to the placenta. Through our evaluation, we found that the type of ionizable lipid and phospholipid are important factors in determining the transfection efficiency of mRNA in BeWos. Specifically, inclusion of C12-200 and DOPE in LNPs increased mRNA transfection in BeWos over other tested lipids. Further, the molar ratio of each lipid component drives intracellular delivery to BeWos *in vitro* and to the placenta *in vivo*. We found that a reduction of PEG molar amount in the LNP was associated with an increase in apparent pKa. Based on our *in vitro* data, this correlation between PEG amount and pKa is associated with improved delivery efficiency. In mice, we found that LNP A10 exhibited biased mRNA delivery to the placenta compared to other LNPs tested. We used this LNP formulation to deliver the more therapeutically relevant PlGF mRNA, which produced serum levels much greater than a normal human pregnancy. Presented herein, we have identified an LNP formulation capable of delivering two mRNA sequences to the placenta, providing an opportunity for treating placental dysfunction.

4. Methods

Formulation of LNPs: C12-200 and DLin-MC3-DMA (MC3) was purchased from MedChem Express (Monmouth Junction, NJ). Other LNP components including cholesterol, DSPC, DOPE, and DMPE-PEG2000 (ammonium salt)) were purchased from Avanti Polar Lipids Inc. (Birmingham, AL). Codon optimized mRNA was prepared by *in vitro* transcription through a collaboration with the Engineered mRNA and Targeted Nanomedicine core facility at the University of Pennsylvania (Philadelphia, PA). Firefly luciferase and PlGF mRNA (transcript variant 1, NM_002632.6) were co-synthesized with 1-methylpseudouridine modifications, and co-transcriptionally capped using the CleanCap system (TriLink) and purified using cellulose based chromatography (PMID: 30933724).

Each LNP was formulated via mixing with micropipettes by combining one volume of lipid/ethanol mixture to three volumes of mRNA in citrate buffer (1:3 ethanol:citrate volume ratio). The lipid mixture for each LNP formulation contained various molar ratios of ionizable lipid:phospholipid:cholesterol:PEG, as indicated in Table S1 mRNA was diluted in citrate buffer (pH 3) to an mRNA:ionizable lipid weight ratio of 1:10 for all LNP formulations. After mixing, the LNPs were dialyzed against PBS (pH 7.4) for 2 h, sterile filtered using 0.2 μm filters, and stored at 4 °C.

Characterization of LNPs: The LNPs in Library A were formulated a total of three separate times to measure consistency in LNP characterization parameters and to complete all experiments. Dynamic light scattering (DLS) measurements and mRNA encapsulation efficiency, as described below, were measured for each LNP formulation in each batch of the library. The average and standard deviation of the hydrodynamic diameter, polydispersity index, and encapsulation efficiency of each LNP is reported for all three batches of the library. Each LNP formulation was diluted 1:100 in deionized water in cuvettes and DLS measurements were run on a Malvern Zetasizer Nano ZS (Malvern Panalytical, Malvern, UK). Samples were diluted 1:100 in deionized water in folded capillary cuvettes and zeta potential was measured in triplicate on the Zetasizer Nano ZS with an applied voltage of 150 V.

The encapsulation efficiency of each LNP formulation was calculated using QuantiFluor® RNA System (Promega, Madison, WI) as previously described [16]. Briefly, LNPs were diluted 1:100 in 1× TE buffer in two microcentrifuge tubes per LNP formulation. 1 % v/v Triton X-100 (Thermo Scientific, Waltham, MA) was added to one of the tubes and both were heated to 37 °C and shaken at 600 RPM for 5 min, followed by cooling to room temperature for 10 min. LNP samples and RNA standards were plated in triplicate in black 96-well plates and the fluorescent reagent was added per the manufacturer instructions. Fluorescent intensity was read on the plate reader (excitation, 492 nm; emission, 540 nm). Background signal was subtracted from each well and triplicate wells for each LNP were averaged. RNA content was quantified by comparing samples to the standard curve, and encapsulation efficiency (%) was calculated according to the equation $EE = \frac{B-A}{B} \times 100$, where A is the RNA content in samples without Triton X-100 treatment (intact LNPs) and B is the RNA content in samples treated with Triton X-100 (lysed LNPs).

The apparent pKa of LNPs was determined via TNS [6-(*p*-toluidinyl) naphthalene-2-sulfonic acid] (Thomas Scientific, Swedesboro, NJ) assays, as previously described [78]. Briefly, a buffer solution of 150 mM sodium chloride, 20 mM sodium phosphate, 20 mM ammonium acetate, and 25 mM ammonium citrate (VWR Chemicals BDH, Radnor, PA) was separated into 21 varied pH solutions, adjusted from pH 2 to 12 in increments of 0.5 pH. 2.5 μL of each LNP formulation was combined with 125 μL of each pH-adjusted solution in black 96-well plates in triplicate. TNS was added to each well for a final TNS concentration of 6 μM and the fluorescence intensity was read on a plate reader (Molecular Devices, San Jose, CA) (excitation, 322 nm; emission, 431 nm). Fluorescence intensity versus pH was plotted, and apparent pKa was calculated as the pH corresponding to 50 % of its maximum value, representing 50 % protonation.

***In vitro* transfection of LNPs with luciferase or PlGF mRNA**: LNPs in the library (A1-A18) were formulated with luciferase mRNA as a reporter molecule and a luciferase assay was performed to measure transfection and mRNA translation in cells. The b30 clone [79] of the BeWo choriocarcinoma cell line (termed "BeWos" herein) were cultured in F–12 K Nutrient Mixture (Kaighn's Mod.) with L-glutamine (Corning Inc., Corning, NY) supplemented with 10 % fetal bovine serum (Avantor, Radnor Township, PA) and 1 % penicillin/streptomycin (VWR, Radnor, PA). Cultures were grown in an incubator set at 37 °C with 5 % CO_2. Cells were plated at 20,000 cells per well in 96-well plates with 200 μL of complete culture media in triplicate for each LNP formulation. After 4 h, cells were treated with LNPs diluted in sterile PBS at 20–100 ng mRNA/well or sterile PBS as the negative control. Luciferase expression was analyzed after 24 h per manufacturer instructions (Promega, Madison, WI). Cells were washed with sterile PBS and 20 μL of 1× lysis buffer was added to each well. After 10 min of incubation at room temperature, cells were centrifuged at 12,000×*g* for 2 min, and lysates were plated into white 96-well plates. 100 μL of luciferase assay substrate was added to each well and the luminescent signal was quantified using the plate reader. The average luminescent signal from each group was normalized to untreated cells and reported as the fold change in luminescence. Statistical analysis of luciferase expression from the LNP library screen was conducted (see "Statistical Analysis" section below).

BeWos were treated with LNPs formulated with PlGF mRNA and free mRNA as described above. After 24 h of incubation with LNPs, cell culture supernatant was collected and centrifuged at 2000×*g* and 4 °C for 5 min to remove cell debris. The supernatant was assayed for PlGF concentration using an enzyme-linked immunosorbent assay (ELISA) per manufacturer instructions (Rockland Immunochemicals, Inc, Pottstown, PA). Briefly, biotinylated anti-human PlGF antibody was used to measure PlGF content in samples via a reaction of avidin-biotin peroxidase complex and 3,3′5,5′-tetramethylbenzidine (TMB) substrate. After color development, stop solution was added to the assay plate and absorbance was read at 450 nm on a microplate reader. Sample absorbance values were compared to a standard curve to calculate PlGF concentration.

LNP Toxicity Analysis: To assess metabolic activity as an indicator of cell viability, BeWos were plated as described above and treated with 100 ng mRNA/well of each LNP formulation. After 24 h, cells were assayed using the MTT (3-(4,5-dimethylthiazol-2-yl)-2,5-diphenyltetrazolium bromide) tetrazolium reduction assay (BioVision, Milpitas, CA) according to manufacturer instructions. Briefly, cells were washed with sterile PBS and 50 μL of serum-free culture media and 50 μL of MTT reagent were added to each well. After incubation for 3 h at 37 °C, 150 μL of MTT solvent was added to each well. The plate was rocked for 15 min at room temperature in the dark and absorbance at 590 nm was read on the plate reader. The average absorbance of wells containing no cells was subtracted as background from each well. The absorbance signal from each group was normalized to untreated cells and reported as the fold change in absorbance.

Administration and Biodistribution of LNPs *In Vivo*: Female mice between 8 and 39 weeks (mean 22.0 weeks) of age were maintained, bred, and used in accordance with Animal Use Protocols approved by the Institutional Animal Care and Use Committee at the University of Delaware (AUP #1320 and #1341). Timed-pregnant CD1 mice were bred and separated 12 h later, denoted as E0.5. At E17.5, dams were injected intravenously via the tail vein with 0.5 mg mRNA/kg mouse of LNPs A3, A10, or A14, or the equivalent volume of saline (n = 3 dam per treatment group). After 4 h, dams were injected intraperitoneally with d-luciferin with potassium salt (150 mg/kg) (Biotium, Fremont, CA). Anesthetized dams were placed supine into the IVIS Lumina III (PerkinElmer, Waltham, MA), and the luminescence signal was detected. Dams were then sacrificed, and the blood was collected via cardiac puncture with a 25-gauge needle and syringe prefilled with 100 μL of

0.5 M EDTA (pH 8). Blood was centrifuged at 2000×*g* at 4 °C for 10 min to separate, and the top plasma layer was transferred into a clean tube and stored at −80 °C. Maternal organs (liver, spleen, pancreas, kidneys, ovaries, heart, and lungs), placentas, and fetuses were excised and imaged separately by IVIS. The weights of all placentas and fetuses were measured via mass balance. Following imaging, maternal organs and placentas were immediately placed on dry ice and stored at −80 °C. Fetal livers were excised from 5 fetuses per dam and immediately placed on dry ice and stored at −80 °C.

Image analysis was conducted in the Living Image software (PerkinElmer, Waltham, MA). To quantify luminescent flux, an ROI was placed over each placenta or dam organ of interest. The average radiance [p/s/cm2/sr] of the ROI with background subtracted for all placentas within each dam were averaged. Next, the average of all of the placentas per replicate dam (n = 3) was calculated. Similarly, the average radiance of the ROI with background subtracted for each dam organ was averaged for the replicate mice (n = 3) treated with each LNP formulation. The liver:placenta and spleen:placenta delivery ratios for each LNP formulation were calculated by dividing the average liver or spleen radiance by the average placental radiance per replicate dam (n = 3), shown with the standard error of the mean.

LNP-Mediated Delivery of PlGF mRNA: Dams (9–23 weeks (mean 13.0 weeks)) at E17.5 were injected via the tail vein with 0.5 mg mRNA/kg mouse weight with free PlGF mRNA, LNPs A3, A10, A14, or the equivalent volume of saline (n = 4 dam per treatment group). Four hours after injection, blood was collected via the submandibular vein of the dam with a 25-gauge needle. Twenty-four hours after injection, dams were sacrificed, and blood was collected via cardiac puncture with a 25-gauge needle and with a syringe prefilled with 100 μL of 0.5 M EDTA (pH 8). Both blood samples were immediately centrifuged after collection at 2000×*g* at 4 °C for 10 min. The top plasma layer was transferred into a clean tube and stored at −80 °C. Placentas and fetuses were excised, rinsed in PBS, and measured using a mass balance. Following measurement, placentas were placed on dry ice and stored at −80 °C. Fetal livers were excised from 5 fetuses per dam and immediately placed on dry ice and stored at −80 °C. Maternal organs (liver, spleen, kidneys, ovaries, lungs, and uterine horn) were surgically excised and immediately placed on dry ice and stored at −80 °C.

The liver and two placentas from each dam were digested to extract protein for PlGF analysis by ELISA. Frozen tissue samples were digested with 300 μL of M-PER digestion reagent (Pierce Biotechnology, Rockford, IL) supplemented with 1× protease and phosphatase inhibitor cocktail (Pierce Biotechnology, Rockford, IL) per 5 mg of tissue on ice. Mechanical grinding of tissues was performed with disposable tissue grinders (Kimble Chase Life Science, Rockwood, TN) per manufacturer instructions. Tissue lysates were kept on ice for 1 h with intermittent 30-s of vortexing and sonication every 15 min. RBC lysis buffer (BioLegend, San Diego, CA) was added to 1× in the lysate solution incubated on ice for 10 min. Lysates were centrifuged at 12,000×*g* for 10 min (4 °C) and the supernatant was transferred to a new tube and stored at −80 °C until analysis. Prior to analysis, lysates were thawed on ice and centrifuged at 12,000×*g* for 10 min (4 °C) to remove debris. Liver, plasma, and placentas were assayed for PlGF concentration using an ELISA per manufacturer instructions, as described above (Rockland Immunochemicals, Inc, Pottstown, PA).

Toxicity Analysis: Liver enzymes ALT and AST were measured using colorimetric assay kits (Cayman Chemical, Ann Arbor, MI) per manufacturer instructions. Briefly, samples and controls were added to the assay plate with substrate and cofactor and incubated at 37 °C for 15 min. Initiator was added to the assay plate and absorbance immediately measured at 340 nm once every minute for 10 min at 37 °C on a microplate reader. The absorbance values were plotted as a function of time and slope was found for the linear portion of the curve. Activity was calculated according to the equation $\text{Activity}\left(\frac{\text{U}}{\text{mL}}\right) = \frac{\frac{\Delta A_{340}}{\text{min}} \times 0.21\text{mL}}{4.11\ \text{mM}^{-1} \times 0.02\text{mL}}$ where activity is ALT or AST activity. ALT and AST assays were performed on fetal liver tissue lysates and in the dam plasma (both prepared as described above). Dam serum and placental tissue lysates (both prepared as described above) were assayed for IL-6 concentration using an ELISA per manufacturer instructions (Invitrogen, Waltham, MA). Sample absorbance values were compared to a standard curve to calculate IL-6 concentration.

Statistical Analysis: Analysis of the DSD was conducted in JMP Pro 16 (SAS Institute Inc., Cary, NC) software using the fit definitive screening platform, while all other analyses were performed using GraphPad Prism 9.0 (San Diego, CA). JMP Pro 16 uses effective model selection for DSDs to identify design variables as active main or pairwise interactions when the p-value computed using the t Ratio and degrees of freedom for error is less than 0.05 [50]. After active effects are identified in the Combined Model Parameter Estimates report, a standard least squares fit is applied to obtain the significant effects in the fit model.

All experiments have n = 3 replicates unless otherwise indicated. Continuous features were assessed for normality using D'Agostino-Pearson omnibus (K2), Anderson-Darling (A2*), Shapiro-Wilk (W), and/or Kolmogorov-Smirnov (distance). Luciferase expression across the different LNPs in Library A, PlGF content in the dam serum and placentas, AST content in the dam serum, number of fetuses and the weights of the fetuses between treatment groups in the *in vivo* study were non-normal. Thus, all were analyzed via the Kruskal-Wallis test followed by pairwise comparisons of the different types of LNPs and/or treatment groups using Dunn's method for multiplicity adjustment. An ordinary one-way ANOVA was used to compare the normally distributed PlGF content in the dam livers, dam ALT and fetal ALT and AST levels, IL-6 content in dam serum and placentas, and the weights of the placentas between treatment groups in the *in vivo* study followed by pairwise comparisons of different types of LNPs adjusted for multiplicity using Tukey's method. Results are represented as mean with standard error of the mean (SEM) and statistical significance was determined at 0.05 (*), 0.01 (**), 0.001 (***), or 0.0001 (****).

Ethics approval and consent to participate

All mice used in the study were maintained, bred, and used in accordance with Animal Use Protocols approved by the Institutional Animal Care and Use Committee at the University of Delaware (AUP #1320 and #1341).

No human subjects or clinical trials research was conducted.

CRediT authorship contribution statement

Rachel E. Young: Conceptualization, Data curation, Formal analysis, Investigation, Methodology, Software, Validation, Writing – original draft, Writing – review & editing. **Katherine M. Nelson:** Data curation, Formal analysis, Investigation, Methodology, Writing – review & editing. **Samuel I. Hofbauer:** Formal analysis, Investigation, Writing – review & editing. **Tara Vijayakumar:** Investigation, Methodology, Writing – review & editing. **Mohamad-Gabriel Alameh:** Investigation, Writing – review & editing. **Drew Weissman:** Investigation, Supervision, Writing – review & editing. **Charalampos Papachristou:** Data curation, Formal analysis, Methodology, Validation, Writing – review & editing. **Jason P. Gleghorn:** Formal analysis, Investigation, Methodology, Supervision, Writing – review & editing, Funding acquisition. **Rachel S. Riley:** Conceptualization, Data curation, Formal analysis, Funding acquisition, Investigation, Methodology, Project administration, Supervision, Validation, Writing – original draft, Writing – review & editing.

Declaration of competing interest

Dr. Rachel Riley is an editorial board member of Bioactive Materials and was not involved in the editorial review or the decision to publish this article. All authors declare that there are no competing interests.

Acknowledgments

Funding:

This work was supported by the New Jersey Health Foundation (PC 44–22); a New Jersey Department of Health grant (COCR22PRG012); the National Science Foundation Graduate Research Fellowship Program (2018266781); the National Institute of Health (T32GM133395 and F31HD105398); and the New Jersey Department of Health Predoctoral Fellowship Program (COCR23PRF027).

Appendix A. Supplementary data

Supplementary data to this article can be found online at https://doi.org/10.1016/j.bioactmat.2023.11.014.

ABBREVIATIONS

LNP	lipid nanoparticle
PEG	polyethylene glycol
DOE	design of experiments
HELLP	hemolysis, elevated liver enzymes, low platelet count
sFlt-1	soluble fms-like tyrosine kinase-1
PlGF	placental growth factor
VEGFR1	vascular endothelial growth factor receptor-1
DSD	definitive screening design
DOPE	1,2-dioleoyl-*sn*-glycero-3-phosphoethanolamine
DSPC	1,2 distearoyl-*sn*-glycero-3-phosphocholine
DMPE-PEG	1,2-dimyristoyl-*sn*-glycero-3-phosphoethanolamine-*N*-[methoxy(polyethylene glycol)-2000] (ammonium salt)
TNS	[6-(*p*-toluidinyl)naphthalene-2-sulfonic acid]
ALT	alanine aminotransferase
AST	aspartate aminotransferase
IL-6	interleukin-6

References

[1] L.A. Jackson, et al., An mRNA vaccine against SARS-CoV-2 - preliminary report, N. Engl. J. Med. 383 (2020) 1920–1931, https://doi.org/10.1056/NEJMoa2022483.
[2] T. Coelho, et al., Safety and efficacy of RNAi therapy for transthyretin amyloidosis, N. Engl. J. Med. 369 (2013) 819–829, https://doi.org/10.1056/NEJMoa1208760.
[3] C.Y. Chen, et al., Treatment of hemophilia A using factor VIII messenger RNA lipid nanoparticles, Mol. Ther. Nucleic Acids 20 (2020) 534–544, https://doi.org/10.1016/j.omtn.2020.03.015.
[4] M.A. Islam, et al., Restoration of tumour-growth suppression in vivo via systemic nanoparticle-mediated delivery of PTEN mRNA, Nat. Biomed. Eng. 2 (2018) 850–864, https://doi.org/10.1038/s41551-018-0284-0.
[5] N. Kong, et al., Synthetic mRNA nanoparticle-mediated restoration of p53 tumor suppressor sensitizes p53-deficient cancers to mTOR inhibition, Sci. Transl. Med. 11 (2019) eaaw1565, https://doi.org/10.1126/scitranslmed.aaw1565.
[6] F. DeRosa, et al., Therapeutic efficacy in a hemophilia B model using a biosynthetic mRNA liver depot system, Gene Ther. 23 (2016) 699–707, https://doi.org/10.1038/gt.2016.46.
[7] B. Truong, et al., Lipid nanoparticle-targeted mRNA therapy as a treatment for the inherited metabolic liver disorder arginase deficiency, Proc. Natl. Acad. Sci. U. S. A. 116 (2019) 21150–21159, https://doi.org/10.1073/pnas.1906182116.
[8] N. Pardi, M.J. Hogan, F.W. Porter, D. Weissman, mRNA vaccines - a new era in vaccinology, Nat. Rev. Drug Discov. 17 (2018) 261–279, https://doi.org/10.1038/nrd.2017.243.
[9] R.S. Riley, C.H. June, R. Langer, M.J. Mitchell, Delivery technologies for cancer immunotherapy, Nat. Rev. Drug Discov. 18 (2019) 175–196, https://doi.org/10.1038/s41573-018-0006-z.
[10] K.A. Hajj, K.A. Whitehead, Tools for translation: non-viral materials for therapeutic mRNA delivery, Nat. Rev. Mater. 2 (2017), https://doi.org/10.1038/natrevmats.2017.56.
[11] L.R. Baden, et al., Efficacy and safety of the mRNA-1273 SARS-CoV-2 vaccine, N. Engl. J. Med. 384 (2021) 403–416, https://doi.org/10.1056/NEJMoa2035389.
[12] F.P. Polack, et al., Safety and efficacy of the BNT162b2 mRNA covid-19 vaccine, N. Engl. J. Med. 383 (2020) 2603–2615, https://doi.org/10.1056/NEJMoa2034577.
[13] D. Adams, et al., Patisiran, an RNAi therapeutic, for hereditary transthyretin amyloidosis, N. Engl. J. Med. 379 (2018) 11–21, https://doi.org/10.1056/NEJMoa1716153.
[14] S. J. Vutrisiran Keam, First approval, Drugs 82 (2022) 1419–1425, https://doi.org/10.1007/s40265-022-01765-5.
[15] X. Hou, T. Zaks, R. Langer, Y. Dong, Lipid nanoparticles for mRNA delivery, Nat. Rev. Mater. 1–17 (2021), https://doi.org/10.1038/s41578-021-00358-0.
[16] R.S. Riley, et al., Ionizable lipid nanoparticles for in utero mRNA delivery, Sci. Adv. 7 (2021) 1–15, https://doi.org/10.1126/sciadv.aba1028.
[17] N. Chaudhary, et al., Lipid nanoparticle structure and delivery route during pregnancy dictates mRNA potency, immunogenicity, and health in the mother and offspring, bioRxiv (2023), https://doi.org/10.1101/2023.02.15.528720, 2023.2002.2015.528720.
[18] P.P.G. Guimaraes, et al., Ionizable lipid nanoparticles encapsulating barcoded mRNA for accelerated in vivo delivery screening, J. Contr. Release 316 (2019) 404–417, https://doi.org/10.1016/j.jconrel.2019.10.028.
[19] A. Akinc, et al., A combinatorial library of lipid-like materials for delivery of RNAi therapeutics, Nat. Biotechnol. 26 (2008) 561–569, https://doi.org/10.1038/nbt1402.
[20] J.A. Kulkarni, D. Witzigmann, J. Leung, Y.Y.C. Tam, P.R. Cullis, On the role of helper lipids in lipid nanoparticle formulations of siRNA, Nanoscale 11 (2019) 21733–21739, https://doi.org/10.1039/c9nr09347h.
[21] X. Cheng, R.J. Lee, The role of helper lipids in lipid nanoparticles (LNPs) designed for oligonucleotide delivery, Adv. Drug Deliv. Rev. 99 (2016) 129–137, https://doi.org/10.1016/j.addr.2016.01.022.
[22] T.M. Allen, P.R. Cullis, Liposomal drug delivery systems: from concept to clinical applications, Adv. Drug Deliv. Rev. 65 (2013) 36–48, https://doi.org/10.1016/j.addr.2012.09.037.
[23] D. Shi, et al., To PEGylate or not to PEGylate: immunological properties of nanomedicine's most popular component, polyethylene glycol and its alternatives, Adv. Drug Deliv. Rev. 180 (2022), 114079, https://doi.org/10.1016/j.addr.2021.114079.
[24] K.J. Kauffman, et al., Optimization of lipid nanoparticle formulations for mRNA delivery in vivo with fractional factorial and definitive screening designs, Nano Lett. 15 (2015) 7300–7306, https://doi.org/10.1021/acs.nanolett.5b02497.
[25] J.E. Dahlman, et al., Barcoded nanoparticles for high throughput in vivo discovery of targeted therapeutics, Proc. Natl. Acad. Sci. U. S. A. 114 (2017) 2060–2065, https://doi.org/10.1073/pnas.1620874114.
[26] Q. Cheng, et al., Selective organ targeting (SORT) nanoparticles for tissue-specific mRNA delivery and CRISPR-Cas gene editing, Nat. Nanotechnol. 15 (2020) 313–320, https://doi.org/10.1038/s41565-020-0669-6.
[27] S.A. Dilliard, Q. Cheng, D.J. Siegwart, On the mechanism of tissue-specific mRNA delivery by selective organ targeting nanoparticles, Proc. Natl. Acad. Sci. U. S. A. 118 (2021), https://doi.org/10.1073/pnas.2109256118.
[28] M. Jayaraman, et al., Maximizing the potency of siRNA lipid nanoparticles for hepatic gene silencing in vivo, Angew Chem. Int. Ed. Engl. 51 (2012) 8529–8533, https://doi.org/10.1002/anie.201203263.
[29] K.A. Hajj, et al., Branched-tail lipid nanoparticles potently deliver mRNA in vivo due to enhanced ionization at endosomal pH, Small 15 (2019), e1805097, https://doi.org/10.1002/smll.201805097.
[30] C.G. Figueroa-Espada, S. Hofbauer, M.J. Mitchell, R.S. Riley, Exploiting the placenta for nanoparticle-mediated drug delivery during pregnancy, Adv. Drug Deliv. Rev. 160 (2020) 244–261, https://doi.org/10.1016/j.addr.2020.09.006.
[31] K.M. Nelson, N. Irvin-Choy, M.K. Hoffman, J.P. Gleghorn, E.S. Day, Diseases and conditions that impact maternal and fetal health and the potential for nanomedicine therapies, Adv. Drug Deliv. Rev. (2020), https://doi.org/10.1016/j.addr.2020.09.013.
[32] K.L. Swingle, et al., Ionizable lipid nanoparticles for in vivo mRNA delivery to the placenta during pregnancy, J. Am. Chem. Soc. 145 (2023) 4691–4706, https://doi.org/10.1021/jacs.2c12893.
[33] G.J. Burton, C.W. Redman, J.M. Roberts, A. Moffett, Pre-eclampsia: pathophysiology and clinical implications, BMJ 366 (2019) l2381, https://doi.org/10.1136/bmj.l2381.
[34] A. Andrikos, et al., Course of the sFlt-1/PlGF ratio in fetal growth restriction and correlation with biometric measurements, feto-maternal Doppler parameters and time to delivery, Arch. Gynecol. Obstet. 305 (2022) 597–605, https://doi.org/10.1007/s00404-021-06186-5.
[35] J.R. Barton, B.M. Sibai, Diagnosis and management of hemolysis, elevated liver enzymes, and low platelets syndrome, Clin. Perinatol. 31 (2004) 807–833, https://doi.org/10.1016/j.clp.2004.06.008, vii.
[36] E. Berzan, R. Doyle, C.M. Brown, Treatment of preeclampsia: current approach and future perspectives, Curr. Hypertens. Rep. 16 (2014) 473, https://doi.org/10.1007/s11906-014-0473-5.
[37] Z. Armaly, J.E. Jadaon, A. Jabbour, Z.A. Abassi, Preeclampsia: novel mechanisms and potential therapeutic approaches, Front. Physiol. 9 (2018) 973, https://doi.org/10.3389/fphys.2018.00973.
[38] C.J. Robinson, D.D. Johnson, E.Y. Chang, D.M. Armstrong, W. Wang, Evaluation of placenta growth factor and soluble Fms-like tyrosine kinase 1 receptor levels in mild and severe preeclampsia, Am. J. Obstet. Gynecol. 195 (2006) 255–259, https://doi.org/10.1016/j.ajog.2005.12.049.
[39] S. Verlohren, et al., The sFlt-1/PlGF ratio in different types of hypertensive pregnancy disorders and its prognostic potential in preeclamptic patients, Am. J. Obstet. Gynecol. 206 (2012) 58 e51–e58, https://doi.org/10.1016/j.ajog.2011.07.037.
[40] C. Saffer, et al., Determination of placental growth factor (PlGF) levels in healthy pregnant women without signs or symptoms of preeclampsia, Pregnancy Hypertens 3 (2013) 124–132, https://doi.org/10.1016/j.preghy.2013.01.004.
[41] H. Zeisler, et al., Predictive value of the sFlt-1:PlGF ratio in women with suspected preeclampsia, N. Engl. J. Med. 374 (2016) 13–22, https://doi.org/10.1056/NEJMoa1414838.

[42] M. Autiero, et al., Role of PlGF in the intra- and intermolecular cross talk between the VEGF receptors Flt 1 and Flk 1, Nat. Med. 9 (2003) 936–943, https://doi.org/10.1038/nm884.
[43] F. Gaccioli, et al., Increased placental sFLT1 (soluble fms-like tyrosine kinase receptor-1) drives the antiangiogenic profile of maternal serum preceding preeclampsia but not fetal growth restriction, Hypertension (2022), https://doi.org/10.1161/HYPERTENSIONAHA.122.19482.
[44] S. Agrawal, S. Shinar, A.S. Cerdeira, C. Redman, M. Vatish, Predictive performance of PlGF (placental growth factor) for screening preeclampsia in asymptomatic women: a systematic review and meta-analysis, Hypertension 74 (2019) 1124–1135, https://doi.org/10.1161/HYPERTENSIONAHA.119.13360.
[45] U.B. Knudsen, et al., A single rapid point-of-care placental growth factor determination as an aid in the diagnosis of preeclampsia, Pregnancy Hypertens 2 (2012) 8–15, https://doi.org/10.1016/j.preghy.2011.08.117.
[46] K. Chau, A. Hennessy, A. Makris, Placental growth factor and pre-eclampsia, J. Hum. Hypertens. 31 (2017) 782–786, https://doi.org/10.1038/jhh.2017.61.
[47] L. Albonici, et al., PlGF immunological impact during pregnancy, Int. J. Mol. Sci. 21 (2020), https://doi.org/10.3390/ijms21228714.
[48] B. Jones, C.J. Nachtsheim, Definitive screening designs with added two-level factors, J. Qual. Technol. 45 (2013).
[49] B. Jones, C.J. Nachtsheim, A class of three-level designs for definitive screening in the presence of second-order effects, J. Qual. Technol. 43 (2011).
[50] B. Jones, C.J. Nachtsheim, Effective design-based model selection for definitive screening designs, Technometrics 59 (2017) 319–329, https://doi.org/10.1080/00401706.2016.1234979.
[51] K.T. Love, et al., Lipid-like materials for low-dose, in vivo gene silencing, Proc. Natl. Acad. Sci. U. S. A. 107 (2010) 1864–1869, https://doi.org/10.1073/pnas.0910603106.
[52] M.A. Oberli, et al., Lipid nanoparticle assisted mRNA delivery for potent cancer immunotherapy, Nano Lett. 17 (2017) 1326–1335, https://doi.org/10.1021/acs.nanolett.6b03329.
[53] K.A. Whitehead, et al., Degradable lipid nanoparticles with predictable in vivo siRNA delivery activity, Nat. Commun. 5 (2014) 4277, https://doi.org/10.1038/ncomms5277.
[54] M. Danaei, et al., Impact of particle size and polydispersity index on the clinical applications of lipidic nanocarrier systems, Pharmaceutics 10 (2018), https://doi.org/10.3390/pharmaceutics10020057.
[55] N. Shobaki, Y. Sato, H. Harashima, Mixing lipids to manipulate the ionization status of lipid nanoparticles for specific tissue targeting, Int. J. Nanomed. 13 (2018) 8395–8410, https://doi.org/10.2147/IJN.S188016.
[56] M.J. Carrasco, et al., Ionization and structural properties of mRNA lipid nanoparticles influence expression in intramuscular and intravascular administration, Commun. Biol. 4 (2021) 956, https://doi.org/10.1038/s42003-021-02441-2.
[57] A. Akinc, et al., Targeted delivery of RNAi therapeutics with endogenous and exogenous ligand-based mechanisms, Mol. Ther. 18 (2010) 1357–1364, https://doi.org/10.1038/mt.2010.85.
[58] B. Shi, et al., Biodistribution of small interfering RNA at the organ and cellular levels after lipid nanoparticle-mediated delivery, J. Histochem. Cytochem. 59 (2011) 727–740, https://doi.org/10.1369/0022155411410885.
[59] B.L. Mui, et al., Influence of polyethylene glycol lipid desorption rates on pharmacokinetics and pharmacodynamics of siRNA lipid nanoparticles, Mol. Ther. Nucleic Acids 2 (2013) e139, https://doi.org/10.1038/mtna.2013.66.
[60] K. Paunovska, et al., A direct comparison of in vitro and in vivo nucleic acid delivery mediated by hundreds of nanoparticles reveals a weak correlation, Nano Lett. 18 (2018) 2148–2157, https://doi.org/10.1021/acs.nanolett.8b00432.
[61] K.A. Whitehead, et al., In vitro - in vivo translation of lipid nanoparticles for hepatocellular siRNA delivery, ACS Nano 6 (2012) 6922–6929.
[62] R.J. Levine, et al., Circulating angiogenic factors and the risk of preeclampsia, N. Engl. J. Med. 350 (2004) 672–683.
[63] D.A. Shah, R.A. Khalil, Bioactive factors in uteroplacental and systemic circulation link placental ischemia to generalized vascular dysfunction in hypertensive pregnancy and preeclampsia, Biochem. Pharmacol. 95 (2015) 211–226, https://doi.org/10.1016/j.bcp.2015.04.012.
[64] M. Zhu, Z. Ren, J.S. Possomato-Vieira, R.A. Khalil, Restoring placental growth factor-soluble fms-like tyrosine kinase-1 balance reverses vascular hyper-reactivity and hypertension in pregnancy, Am. J. Physiol. Regul. Integr. Comp. Physiol. 311 (2016) R505–R521, https://doi.org/10.1152/ajpregu.00137.2016.
[65] H. Parhiz, et al., Added to pre-existing inflammation, mRNA-lipid nanoparticles induce inflammation exacerbation (IE), J. Contr. Release 344 (2021) 50–61, https://doi.org/10.1016/j.jconrel.2021.12.027.
[66] M.G. Alameh, et al., Lipid nanoparticles enhance the efficacy of mRNA and protein subunit vaccines by inducing robust T follicular helper cell and humoral responses, Immunity 54 (2021) 2877–2892 e2877, https://doi.org/10.1016/j.immuni.2021.11.001.
[67] H. Parhiz, et al., PECAM-1 directed re-targeting of exogenous mRNA providing two orders of magnitude enhancement of vascular delivery and expression in lungs independent of apolipoprotein E-mediated uptake, J. Contr. Release 291 (2018) 106–115, https://doi.org/10.1016/j.jconrel.2018.10.015.
[68] P.M. Coan, et al., Adaptations in placental nutrient transfer capacity to meet fetal growth demands depend on placental size in mice, J. Physiol. 586 (2008) 4567–4576, https://doi.org/10.1113/jphysiol.2008.156133.
[69] C.E. Hayward, et al., Placental adaptation: what can we learn from birthweight: placental weight ratio? Front. Physiol. 7 (2016) 28, https://doi.org/10.3389/fphys.2016.00028.
[70] N.S. Irvin-Choy, K.M. Nelson, M.N. Dang, J.P. Gleghorn, E.S. Day, Gold nanoparticle biodistribution in pregnant mice following intravenous administration varies with gestational age, Nanomedicine 36 (2021), 102412, https://doi.org/10.1016/j.nano.2021.102412.
[71] H. Suzuki, et al., Effect of recombinant placental growth factor 2 on hypertension induced by full-length mouse soluble fms-like tyrosine kinase 1 adenoviral vector in pregnant mice, Hypertension 54 (2009) 1129–1135, https://doi.org/10.1161/HYPERTENSIONAHA.109.134668.
[72] F.T. Spradley, et al., Placental growth factor administration abolishes placental ischemia-induced hypertension, Hypertension 67 (2016) 740–747, https://doi.org/10.1161/HYPERTENSIONAHA.115.06783.
[73] A. Makris, et al., Placental growth factor reduces blood pressure in a uteroplacental ischemia model of preeclampsia in nonhuman primates, Hypertension 67 (2016) 1263–1272, https://doi.org/10.1161/HYPERTENSIONAHA.116.07286.
[74] K. McLaughlin, et al., PlGF (placental growth factor) testing in clinical practice: evidence from a Canadian tertiary maternity referral center, Hypertension 77 (2021) 2057–2065, https://doi.org/10.1161/HYPERTENSIONAHA.121.17047.
[75] A.C.M. Kluivers, et al., Angiogenic imbalance in pre-eclampsia and fetal growth restriction: enhanced soluble Fms-like tyrosine kinase-1 binding or diminished production of placental growth factor? Ultrasound Obstet. Gynecol. (2022) https://doi.org/10.1002/uog.26088.
[76] T. Odorisio, et al., Mice overexpressing placenta growth factor exhibit increased vascularization and vessel permeability, J. Cell Sci. 115 (2002) 2559–2567.
[77] A. Adini, T. Kornaga, F. Firoozbakht, L.E. Benjamin, Placental growth factor is a survival factor for tumor endothelial cells and macrophages, Cancer Res. 62 (2002) 2749–2752.
[78] J. Heyes, L. Palmer, K. Bremner, I. MacLachlan, Cationic lipid saturation influences intracellular delivery of encapsulated nucleic acids, J. Contr. Release 107 (2005) 276–287, https://doi.org/10.1016/j.jconrel.2005.06.014.
[79] B. Wice, D. Menton, H. Geuze, A.L. Schwartz, Modulators of cyclic AMP metabolism induce syncytiotrophoblast formation in vitro, Exp. Cell Res. 186 (1990) 306–316.